Supporting Information: Quantum Engineering of Helical Charge Migration in HCCI

ChunMei Liu(刘春梅)[1], Jörn Manz(源满)[2,3,4*], Huihui Wang(王慧慧)[3,4], Yonggang Yang(杨勇刚)[3,4**]

[1] *Crystal Physics Research Center, College of Science, Nanjing University of Posts and Telecommunications, Nanjing 210023, China*

[2] *Institut für Chemie und Biochemie, Freie Universität Berlin, 14195 Berlin, Germany*

[3] *State Key Laboratory of Quantum Optics and Quantum Optics Devices, Institute of Laser Spectroscopy, Shanxi University, Taiyuan 030006, China;*

[4] *Collaborative Innovation Center of Extreme Optics, Shanxi University, Taiyuan 030006, China*

I. Quantum chemical calculations of the electronic eigenfunctions, eigenenergies, the one-electron density matrix elements and the transition dipole matrix elements of the oriented HCCI

The electronic eigenfunctions Ψ_j and eigenenergies E_j of iodo acetylene HCCI oriented along the z-axis are calculated as solutions of the time-independent Schrödinger equation (TISE) $H_e\Psi_j = E_j\Psi_j$. The Hamiltonian H_e accounts for the kinetic energy of the electrons, and for the Coulomb interactions of all electrons and the nuclei. The nuclear structure is frozen as shown in Fig. 1(a). It is adapted from Ref. [1] where it has been calculated by means of the coupled clusters singles doubles (triples)[2] method (CCSD(T)/cc-pVQZ*). Here cc-pVQZ* means Dunning's correlation consistent basis set with polarization functions for the valence electrons up to the quintuple-zeta level for all atoms.[3] The star indicates the use of proper pseudo-potentials and the corresponding pseudo-potential basis set ("cc-pVQZ-pp") for iodine.[4] We focus on just five eigenfunctions, namely Ψ_0 for the ground state with irreducible representation (IRREP) Σ^+, and the degenerate pairs Ψ_{1x}, Ψ_{1y} and Ψ_{2x}, Ψ_{2y} for the first and second excited Π states. For convenience, the eigenfunctions are also denoted by their IRREPs, i.e. we set $\Psi_0 = 1\Sigma^+$, $\Psi_{1x} = 1\Pi_x$, $\Psi_{1y} = 1\Pi_{1y}$, $\Psi_{2x} = 2\Pi_x$, $\Psi_{2y} = 2\Pi_y$. They depend on the spatial ($\mathbf{r}_n$) and spin (α_n or β_n) coordinates of $N = 16$ valence electrons, $n = 1, 2, ..., N$. In short-hand notation, they are written as $\Psi_j(\mathbf{r}_1, \mathbf{r}_2, ..., \mathbf{r}_N)$, without explicit notation of the spins.

The TISE is solved by means of the state averaged complete active state self-consistent field method[5] (CASSCF(16,13)/cc-pVQZ*) for all atoms, as implemented in MOLPRO.[6] For convenience, these calculations assume C_{2v} symmetry of HCCI. Subsequently, the resulting IRREPs of the wavefunctions are re-assigned to $C_{\infty v}$ symmetry, in particular $A_1 \to \Sigma^+$ for the ground state and $B_1 \to \Pi_x$, $B_2 \to \Pi_y$ for the degenerate excited Π states.

Using the eigenfunctions $\Psi_j(\mathbf{r}_1, \mathbf{r}_2, ..., \mathbf{r}_N)$, we employ the ORBKIT package[7–9] to calculate the corresponding diagonal and off-diagonal matrix elements of the one-electron density,

$$\begin{aligned}\rho_{ij}(\mathbf{r}) &= \int ... \int \psi_i(\mathbf{r}_1, \mathbf{r}_2, ..., \mathbf{r}_N)\psi_j(\mathbf{r}_1, \mathbf{r}_2, ..., \mathbf{r}_N) \sum_{n=1}^{N} \delta(\mathbf{r} - \mathbf{r}_n) d\mathbf{r}_1 d\mathbf{r}_2 ... d\mathbf{r}_N \\ &= N \int ... \int \psi_i(\mathbf{r}, \mathbf{r}_2, ..., \mathbf{r}_N)\psi_j(\mathbf{r}, \mathbf{r}_2, ..., \mathbf{r}_N) d\mathbf{r}_2 d\mathbf{r}_3 ... d\mathbf{r}_N.\end{aligned} \tag{S1}$$

Using the $\rho_{ij}(\mathbf{r})$, the transition dipole matrix elements $\mathbf{d}_{ij}$ for the transitions between states i and j are calculated as

$$\mathbf{d}_{ij} = -e \cdot \int \mathbf{r}\rho_{ij}(\mathbf{r}) d\mathbf{r}. \tag{S2}$$

The corresponding permanent dipoles $\mathbf{d}_{jj}$ of the oriented HCCI in state j are calculated by MOLPRO.

The resulting energy levels of the ground state $1\Sigma^+$ and the degenerate excited states $1\Pi_x, 1\Pi_y$ and $2\Pi_x, 2\Pi_y$ are 0.00 eV, 5.60 eV and 7.88 eV, respectively. The values of the non-zero components of the permanent dipoles

*Electronic address: (Yang Y) ygyang@sxu.edu.cn;(Manz J) jmanz@chemie.fu-berlin.de

and the transition dipole matrix elements for the symmetry allowed transitions between these states are

$$\begin{aligned}
&(d_z)_{00} = -0.0115ea_0, (d_z)_{1x,1x} = (d_z)_{1y,1y} = -0.9237ea_0, \\
&(d_z)_{2x,2x} = (d_z)_{2y,2y} = -1.6994ea_0, (d_x)_{0,1x} = (d_y)_{0,1y} = 0.3164ea_0, \\
&(d_x)_{0,2x} = (d_y)_{0,2y} = 0.1163ea_0, (d_z)_{1x,2x} = (d_z)_{1y,2y} = 1.2418ea_0.
\end{aligned} \tag{S3}$$

II. Quantum simulations of the laser driven electron dynamics of the oriented HCCI

The laser driven electron dynamics of the oriented HCCI is represented by the time-dependent electronic wavefunction $\Psi(t)$. It is calculated, in semiclassical dipole ($\hat{\mathbf{d}}$) approximation, as solution of the time-dependent Schrödinger equation (TDSE)

$$i\hbar\frac{\partial\Psi(t)}{\partial t} = H(t)\Psi(t) \tag{S4}$$

with Hamiltonian

$$\boldsymbol{H}(t) = \boldsymbol{H}_e - \hat{\mathbf{d}}\cdot\boldsymbol{\epsilon}(t) = \boldsymbol{H}_e - \hat{d}_x\epsilon_x(t) - \hat{d}_y\epsilon_y(t) - \hat{d}_z\epsilon_z(t), \tag{S5}$$

where $\boldsymbol{\epsilon}(t) = \boldsymbol{\epsilon}_{\rm I}(t)$ or $\boldsymbol{\epsilon}(t) = \boldsymbol{\epsilon}_{\rm II}(t)$ is the electric field of the laser pulses for strategy I or II, respectively, cf. eqns. (1), (2) of the main text. Note that $\boldsymbol{\epsilon}_{{\rm II},z}(t) = 0$ because strategy II uses circularly polarized laser pulses, exclusively. The TDSE (S4) is solved subject to the initial ($t = t_i = -5$ fs) condition

$$\Psi(t_i) = \Psi_0 \tag{S6}$$

representing the HCCI molecule in its electronic ground state. Subsequently, the laser pulses excite the molecule, partially to

$$\psi_1 = \frac{1}{\sqrt{2}}\left(\psi_{1x} + i\psi_{1y}\right), \psi_2 = \frac{1}{\sqrt{2}}\left(\psi_{2x} + i\psi_{2y}\right). \tag{S7}$$

The wavefunction is, therefore, written as

$$\Psi(t) = c_0(t)\Psi_0 + c_1(t)\Psi_1 + c_2(t)\Psi_2. \tag{S8}$$

In principle, one may include additional electronic eigenfunctions in the expansion (S8), but this is not necessary, for two reasons: First, according to our calculations there are only few additional eigenstates within the spectral widths ($= \hbar/2\tau$) of the transform-limited laser pulses but none of them has proper components of the transition dipoles as requested in Fig. 1 (For example, they may have non-zero z-components while non-zero x, y-components are needed, or vice versa.) Second, in view of the small populations of the excited states, we assume that ladder climbing to even more excited states is negligible. The restriction of the expansion (S8) to just three states implies that the corresponding probabilities of occupying states $j = 0, 1, 2$

$$P_j(t) = |c_j(t)|^2 \tag{S9}$$

are normalized,

$$\sum_{j=0}^{2} P_j(t) = 1. \tag{S10}$$

Using the Ansatz (S8), the TDSE (S4) can be rewritten as differential equation for the vector of the coefficients $\boldsymbol{c}(t) = (\boldsymbol{c}_0(t), \boldsymbol{c}_1(t), \boldsymbol{c}_2(t))^T$ (see e. g. Refs.[10,11])

$$i\hbar\frac{d\boldsymbol{c}(t)}{dt} = \boldsymbol{H}(t)\boldsymbol{c}(t). \tag{S11}$$

The nine matrix elements of the 3×3 Hamilton matrix $\hat{\boldsymbol{H}}(t)$ are

$$H_{ij}(t) = H_{e,ij} - \boldsymbol{d}_{ij}\cdot\boldsymbol{\epsilon}(t), \tag{S12}$$

which consists of the diagonal term for the electronic energies,

$$H_{e,ij} = E_i\delta_{ij} \tag{S13}$$

and the terms for the laser-dipole couplings, cf. eqn. (S3).

The algebraic version of the TDSE (S11) is solved by means of the simple Euler method for the interaction picture, as in Ref.[10]. Converged results are obtained for the equidistant time step, $\Delta t = 0.001$ fs.

III. Determination of the parameters of optimal laser pulses for quantum engineering of helical charge migration in oriented HCCI

The TDSE (S4) and the algebraic version (S11) are valid for a large variety of laser pulses which induce helical charge migration (HCM) in the oriented HCCI, according to the strategies I or II. Here we present quantum engineering of HCM for an illuminating example which demonstrates the equivalence of the two different approaches. For this purpose, the laser pulses must be designed such that for both cases I and II, they drive the electronic wavefunction from the initial ground state (S6) to the same target state for HCM,

$$\Psi(t_f) = c_0(t_f)\Psi_0 + c_1(t_f)\Psi_1 + c_2(t_f)\Psi_2 \tag{S14}$$

at the end ($t = t_f = 5$fs) of the laser pulse. For the present example, the target coefficients are chosen rather arbitrarily to be real-valued,

$$c_j(t_f) \equiv C_j = \sqrt{P_j}(t_f) \tag{S15}$$

with probabilities

$$P_0(t_f) = 0.97, P_1(t_f) = 0.02, P_2(t_f) = 0.01. \tag{S16}$$

Subsequently, for times $t' = t - t_f > 0$, the electronic wavefunction

$$\Psi(t') = C_0\Psi_0 + C_1 e^{-iE_1 t'/\hbar}\Psi_1 + C_2 e^{-iE_2 t'/\hbar}\Psi_2 \tag{S17}$$

represents HCM, as shown in the main text, cf. Figs. 3.

The analytical form of the laser pulses is specified in the main text, cf. eqns. (1), (2). Here we present the method for determining the laser parameters $lp = \{\epsilon, \tau, \omega, \eta\}$ of the individual pulses such that they yield the same HCM (S17) by means of strategies I and II. It has four steps:

(i) We use resonant frequencies such that

$$\hbar\omega_{ij} = E_j - E_i. \tag{S18}$$

(ii) The durations of the pulses are set equal to a rather small value, to support the present scenario of frozen nuclei.[1,10]

$$\tau_{01} = \tau_{12} = \tau_{02} \equiv \tau = 2.5fs. \tag{S19}$$

(iii) Next, the amplitudes of the electric fields are determined such that the laser pulses yield the same target probabilities (S16) for both strategies I and II. In principle, this can be achieved by means of brute force scans of the amplitudes versus the resulting probabilities. Alternatively, we use an illuminating two (sub-)step approach. The first sub-step determines reasonable approximations. The second sub-step starts from the approximations and determines neighboring values for perfect quantum control, by systematic fine-tuning.

Specifically, the first sub-step makes use of the fact that strategies I and II employ superpositions of two laser pulses which should induce specific transitions between two electronic eigenstates of the oriented HCCI. The literature has simple rules for the field strength of laser pulses with Gaussian envelopes which achieve the target transitions between two states.[10,12] These rules have been derived by means of the rotating wave approximation, and they are employed here as zero-order approximations for our purposes. For example, for strategy I, the right (+) circularly polarized laser pulse should transfer about 0.03 population from Ψ_0 to Ψ_1. For this purpose, the approximate value of the field amplitude $\epsilon_{01,I}$ should satisfy the condition $\sin^2(\sqrt{\pi}\epsilon_{01,I}(d_x)_{0,1x}\tau_{01}/\sqrt{2}\hbar) = 0.03$.[10] The linearly z-polarized laser pulse of strategy I should transfer 1/3 of the population from Ψ_1 to Ψ_2. Accordingly, the approximate value of the field amplitude $\epsilon_{12,I}$ should satisfy the condition[10,12] $\sin^2(\sqrt{\pi}\epsilon_{12,I}(d_z)_{1x,2x}\tau_{12}/2\hbar) = 1/3$. Likewise, for strategy II, the two right (+) circularly polarized pulses should transfer $P_1(t_f) = 0.02$ and $P_2(t_f) = 0.01$ populations from Ψ_0 to Ψ_1 and from Ψ_0 to Ψ_2; for these purposes, the corresponding field strengths should satisfy the conditions $\sin^2(\sqrt{\pi}\epsilon_{01,II}(d_x)_{0,1x}\tau_{01}/\sqrt{2}\hbar) = 0.02$ and $\sin^2(\sqrt{\pi}\epsilon_{02,II}(d_x)_{0,2x}\tau_{02}/\sqrt{2}\hbar) = 0.01$, respectively.[10] Starting from the approximate values $\epsilon_{01,I}, \epsilon_{12,I}$ and $\epsilon_{01,II}, \epsilon_{02,II}$, the second sub-step then yields close-lying values $\epsilon_{01,I}$ for

perfect quantum control of the target populations. The values of the target field strengths are listed in Table SI-1.

(iv) Finally, the carrier envelope phases (CEP) are determined such that they yield the real-valued coefficients (S15). Again, in principle, this can be achieved by means of brute force scans of the CEPs versus the resulting phases of the coefficients. Alternatively, we use an efficient two (sub-)step approach. Specifically for strategy I, we vary η_{01} in the domain $[0, 2\pi]$ till we obtain the same phases for the coefficients $c_0(t_f)$ and $c_1(t_f)$. Subsequently, we vary η_{12} till we obtain the same phases for the coefficients $c_1(t_f)$ and $c_2(t_f)$. This way, we arrive at coefficients $c_0(t_f), c_1(t_f), c_2(t_f)$ which possess the same (irrelevant) global phase; the latter can be re-set to zero, such that the coefficients are real-valued and positive.

Likewise for strategy II, we vary η_{01} and η_{02} independently till we obtain the same phase for all coefficients $c_0(t_f), c_1(t_f)$ and $c_2(t_f)$. This global phase is then set equal to zero, i.e. the coefficients are real-valued and positive. The resulting CEPs for perfect quantum control by equivalent strategies I and II are also listed in Table SI-1.

Table SI- 1: Laser parameters $lp = \{\epsilon, \tau, \omega, \eta\}$ for quantum engineering of helical charge migration in oriented HCCI[a]

Strategy	target $\rightarrow$ transition[b]	polarization[c]	ϵ/(GV/m)	τ/fs	$\hbar\omega$/eV[d]	T/fs[e]	η
I	$\Psi_0 \rightarrow \Psi_1$	circular	2.345	2.5	5.60	0.74	$\pi - 0.103$
I	$\Psi_1 \rightarrow \Psi_2$	linear	5.578	2.5	2.28	1.81	$\pi + 0.002$
II	$\Psi_0 \rightarrow \Psi_1$	circular	1.792	2.5	5.60	0.74	$\pi - 0.101$
II	$\Psi_0 \rightarrow \Psi_2$	circular	3.446	2.5	7.88	0.53	$\pi + 1.420$

[a] cf. eqns. (1),(2) in main text. The corresponding maximum intensities of the laser pulses for strategies I and II are 9.725 and 4.007 TW/cm^2, respectively. ϵ =field amplitude, τ =duration, ω =carrier frequency, η =carrier envelope phase CEP.

[b] $\Psi_0 = 1\Sigma^+, \Psi_1 = (1\Pi_x + i \cdot 1\Pi_y)/\sqrt{2}, \Psi_2 = (2\Pi_x + i \cdot 2\Pi_y)/\sqrt{2}$.

[c] circular = right (+) circularly polarized, linear = linearly z-polarized.

[d] resonant photon energy, $\hbar\omega_{ij} = E_j - E_i$.

[e] period $T_{ij} = 2\pi/\omega_{ij}$.

IV. Time-dependent one-electron density matrices and dipoles documenting helical charge migration in HCCI after the laser control

The electronic wavefunction (S17) represents helical charge migration in the oriented HCCI for the time after the laser pulse, $t' = t - t_f > 0$. This is illustrated in Figs. 3 and SI-1 by the time-dependent dipole $\hat{\mathbf{d}}(t')$ and by snapshots of the one-electron density difference $\Delta\rho(t')$, respectively. This Section explains the methods for calculating $\Delta\rho(t')$ and $\hat{\mathbf{d}}(t')$.

The wavefunction (S17) yields the time-dependent N-electron density

$$
\begin{aligned}
\tilde{\rho}(t') &= \psi(t')\psi^*(t') \\
&= C_0^2\psi_0\psi_0^* + C_1^2\psi_1\psi_1^* + C_2^2\psi_2\psi_2^* + C_0C_1\left(\psi_0\psi_1^* e^{i\omega_{01}t'} + \psi_0^*\psi_1 e^{-i\omega_{01}t'}\right) \\
&+ C_0C_2\left(\psi_0\psi_2^* e^{i\omega_{02}t'} + \psi_0^*\psi_2 e^{-i\omega_{02}t'}\right) + C_1C_2\left(\psi_1\psi_2^* e^{i\omega_{21}t'} + \psi_1^*\psi_2 e^{-i\omega_{21}t'}\right) \\
&= C_0^2\psi_0^2 + \frac{C_1^2}{2}\left(\psi_{1x}^2 + \psi_{1y}^2\right) + \frac{C_2^2}{2}\left(\psi_{2x}^2 + \psi_{2y}^2\right) + \sqrt{2}C_0C_1[\psi_0\psi_{1x}\cos(\omega_{01}t') + \psi_0\psi_{1y}\sin(\omega_{01}t')] \\
&+ \sqrt{2}C_0C_2\left[\psi_0\psi_{2x}\cos(\omega_{02}t') + \psi_0\psi_{2y}\sin(\omega_{02}t')\right] \\
&+ C_1C_2\left[(\psi_{1x}\psi_{2x} + \psi_{1y}\psi_{2y})\cos(\omega_{21}t') + (\psi_{1x}\psi_{2y} - \psi_{1y}\psi_{2x})\sin(\omega_{21}t')\right].
\end{aligned}
\tag{S20}
$$

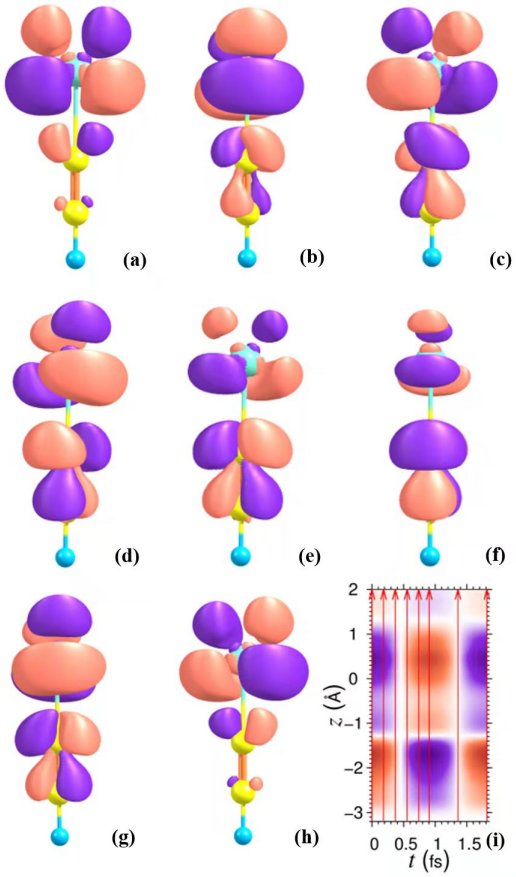

Fig. SI-1. Helical charge migration (HCM) of HCCI oriented along the laboratory z-axis, for times $t' = t - t_f > 0$ after the end ($t_f = 5$ fs) of the laser pulses for strategy I (cf. Figs. 1(c) and 2) or for strategy II (cf. Figs. 1(c) and 4). (a)-(h) Snapshots of the one-electron density difference $\Delta\rho(t') = \rho(t') - \bar{\rho}$ between the density at t' and the mean density. Domains with enhanced ($\Delta\rho(t') > 0$) and with diminished ($\Delta\rho(t') < 0$) densities are represented by orange- and purple-colored lobes, respectively. HCCI oriented along the z-axis is illustrated by a stick-and-ball cartoon, cf. Fig. 1(a). The scaling is the same in all panels (a)-(i), with the center-of-mass at $z = 0$. The snapshots (a)-(e) are at times $t' = k \cdot T_{01}/4, k = 0, 1, .., 4$ with $T_{01} = h/(E_1 - E_0) = 0.74$ fs. They illustrate the circular charge migration (CCM) as component of HCM. Snapshots (a), (f), (g), (h) are at times $t' = k \cdot T_{12}/4, k = 0, 2, 3, 4$ with $T_{12} = h/(E_2 - E_1) = 1.81$ fs, during linear charge migration (LCM), the other building-stone of HCM. (i) The LCM component of HCM is documented by the contour plot of $\Delta\rho_z(z, t') = \int\int dxdy\Delta\rho(x, y, z, t')$. The sequence of eight vertical arrows marks the times for the snapshots (a)-(h).

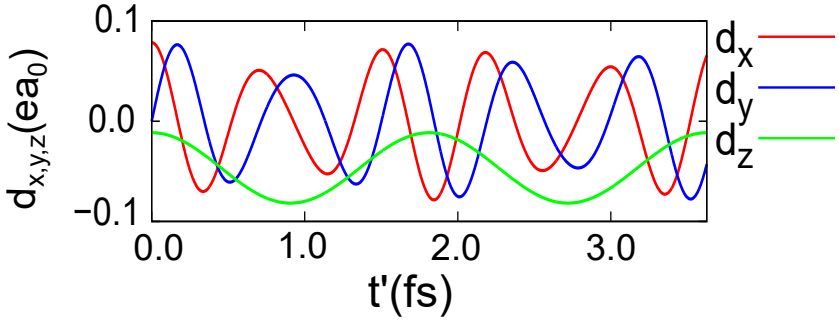

Fig. SI-2. The components $d_x(t'), d_y(t'), d_z(t')$ of the helical dipole $\mathbf{d}(t')$ shown in Fig.3. The $x-$ and $y-$ components document quasi-periodic CCM with the quasi-periodic circular charge migration (CCM) component of HCM, with $T_{01} = 0.74$ fs. The z-component documents periodic linear charge migration (LCM) component of HCM, with period $T_{12} = 1.81$ fs.

This in turn yields the time-dependent one-electron density

$$\begin{aligned}\rho(\mathbf{r},t') &= \int ... \int \tilde{\rho}(\mathbf{r}_1,\mathbf{r}_2,...,\mathbf{r}_N,t') \sum_{n=1}^{N} \delta(\mathbf{r}-\mathbf{r}_i) d\mathbf{r}_1 d\mathbf{r}_2 ... d\mathbf{r}_N \\ &= N \int ... \int \tilde{\rho}(\mathbf{r},\mathbf{r}_2,...,\mathbf{r}_N,t) d\mathbf{r}_2 d\mathbf{r}_3 ... d\mathbf{r}_N \\ &= C_0^2\rho_{00} + \frac{C_1^2}{2}(\rho_{1x,1x}+\rho_{1y,1y}) + \frac{C_2^2}{2}(\rho_{2x,2x}+\rho_{2y,2y}) \\ &+ \sqrt{2}C_0C_1\left[\rho_{0,1x}\cos(\omega_{01}t') + \rho_{0,1y}\sin(\omega_{01}t')\right] \\ &+ \sqrt{2}C_0C_2\left[\rho_{0,2x}\cos(\omega_{02}t') + \rho_{0,2y}\sin(\omega_{02}t')\right] \\ &+ C_1C_2\left[(\rho_{1x,2x}+\rho_{1y,2y})\cos(\omega_{21}t') + (\rho_{1x,2y}-\rho_{1y,2x})\sin(\omega_{21}t')\right].\end{aligned} \tag{S21}$$

The time-averaged mean value of $\rho(\mathbf{r},t')$ is

$$\bar{\rho}(\mathbf{r}) = C_0^2\rho_{00} + \frac{C_1^2}{2}\left(\rho_{1x,1x}+\rho_{1y,1y}\right) + \frac{C_2^2}{2}\left(\rho_{2x,2x}+\rho_{2y,2y}\right). \tag{S22}$$

From eqns. (S23) and (S24) we obtain the time-dependent density difference

$$\Delta\rho(\mathbf{r},t') = \rho(\mathbf{r},t') - \bar{\rho}(\mathbf{r}) \tag{S23}$$

documented by snapshots in Fig. SI-1.

Contour plots SI-1(a) - SI-1(e) of $\Delta\rho(t')$ illustrate the CCM component of HCM around the molecular axis. Contour plots SI-1(a), SI-1(f) - SI-1(h) are taken during LCM from the C-I bond to the C=C bond, and back. The contour plot of $\Delta\rho_z(z,t') = \int\int dxdy\Delta\rho(x,y,z,t')$ in panel 3(i) documents LCM quantitatively, as in Refs. [10,13].

Finally, the time-dependent dipole moment is calculated using the time-dependent one-electron density $\rho(\mathbf{r},t')$ and the time-independent charge density $\rho_c(\mathbf{r})$ of the system formed by all the nuclei and all the core electrons,

$$\begin{aligned}\mathbf{d}(t') = -e\cdot\int \mathbf{r}\rho(\mathbf{r},t')d\mathbf{r} + \int \mathbf{r}\rho_c(\mathbf{r})d\mathbf{r} &= C_0^2\mathbf{d}_{00} + \frac{C_1^2}{2}\left(\mathbf{d}_{1x,1x}+\mathbf{d}_{1y,1y}\right) + \frac{C_2^2}{2}\left(\mathbf{d}_{2x,2x}+\mathbf{d}_{2y,2y}\right) \\ &+ \sqrt{2}C_0C_1\left[\mathbf{d}_{0,1x}\cos(\omega_{01}t') + \mathbf{d}_{0,1y}\sin(\omega_{01}t')\right] \\ &+ \sqrt{2}C_0C_2\left[\mathbf{d}_{0,2x}\cos(\omega_{02}t') + \mathbf{d}_{0,2y}\sin(\omega_{02}t')\right] \\ &+ C_1C_2\left[(\mathbf{d}_{1x,2x}+\mathbf{d}_{1y,2y})\cos(\omega_{21}t') + (\mathbf{d}_{1x,2y}-\mathbf{d}_{1y,2x})\sin(\omega_{21}t')\right].\end{aligned} \tag{S24}$$

Using eqn. (S3), (S15), (S16), this yields the time evolution of the Cartesian components of the dipole, as illustrated in Fig. SI-2.

$$\begin{aligned}d_x(t')/ea_0 &= 0.0623\cos(\omega_{01}t') + 0.0162\cos(\omega_{02}t') \\ d_y(t')/ea_0 &= 0.0623\sin(\omega_{01}t') + 0.0162\sin(\omega_{02}t') \\ d_z(t')/ea_0 &= -0.0466 + 0.0351\cos(\omega_{21}t').\end{aligned} \tag{S25}$$

The corresponding helical path of $\mathbf{d}(t')$ is shown in Fig. 3, mapping helical charge migration in the oriented HCCI.

V. On the equivalence of the strategies I and II for quantum engineering of helical charge migration in oriented HCCI

The equivalence of the quantum strategies I and II rests on the fact that they yield the same wavefunction (3), for times $t' = t - t_f > 0$. This is because they yield the same coefficients $c_j(t_f)$ at the end of the laser pulses. The subsequent coherent quantum dynamics proceeds without any memory - it does not depend on the strategies for preparing the $c_j(t_f)$. Specifically, strategy I transfers population from the ground state $j = 0$

to the two excited states $j = 1$ and 2, by laser-induced transitions $0 \rightarrow 1$ and $1 \rightarrow 2$. In contrast, strategy II achieves the same effect by transitions $0 \rightarrow 1$ and $0 \rightarrow 2$. The symmetry selection rules for the transitions require that the linearly polarized pulse for $1 \rightarrow 2$ (strategy I) has to be substituted by the circularly polarized pulse for $0 \rightarrow 2$ (strategy II).

References

[1] Kraus P M, Mignolet B, Baykusheva D, Rupenyan A, Horný L, et al. 2015 *Science* **350** 790-795.
[2] Deegan M J O and Knowles P J 1994 *Chem. Phys. Lett.* **227** 321-326.
[3] Dunning Jr. T H 1989 *J. Chem. Phys.* **90** 1007.
[4] Peterson K A, Shepler B C, Figgen D and Stoll H 2006 *J. Phys. Chem. A* **110** 13877.
[5] Knowles P J and Wörner H-J 1985 *Chem. Phys. Lett.* **115** 259.
[6] Wörner H-J, et al. MOLPRO, version 2012.1, A package of ab initio programs. http://www.molpro.net, 2012.
[7] Hermann G, Pohl V, Tremblay J C, Paulus B, Hege H -C and Schild A 2016 *J. Comput. Chem.* **37** 1511-1520.
[8] Hermann G, Pohl V and Tremblay J C 2017 *J. Comput. Chem.* **38** 2378-2387.
[9] Pohl V, Hermann G and Tremblay J C 2017 *J. Comput. Chem.* **38** 1515-1527.
[10] Jia D, Manz J and Yang Y 2017 *J. Mod. Opt.* **64** 960.
[11] Barth I and Manz J 2006 *Angew. Chem. Int. Ed.* **45** 2962-2965.
[12] Liu C, Manz J and Yang Y 2015 *ChemPhysChem* **16** 191.
[13] Jia D, Manz J and Yang Y 2019 *J. Phys. Chem. Lett.* **10** 4273.